J. H. Walther
Postdoctoral Fellow
e-mail: walther@inf.ethz.ch

P. Koumoutsakos[1]
Professor
e-mail: petros@inf.ethz.ch

Institute of Computational Sciences,
ETH Zentrum,
Weinbergstrasse 43,
CH-8092 Zürich, Switzerland

Molecular Dynamics Simulation of Nanodroplet Evaporation

Molecular dynamics simulations are used to study the sub-critical evaporation of a nanometer-size droplet at 300 K and 3 MPa. Classical molecular dynamics techniques are combined with an adaptive tree data structure for the construction of the neighbor lists, allowing efficient simulations using hundreds of thousands of molecules. We present a systematic convergence study of the method demonstrating its convergence for heat conduction problems in submicron scales. These high resolution simulations compute values of the evaporation coefficient that are in excellent agreement with theoretical predictions. [DOI: 10.1115/1.1370517]

Keywords: Nanofluidics, Nanodroplet, Molecular Dynamics Simulation

1 Introduction

Phenomena associated with droplet dynamics are of fundamental importance to non-premixed combustion studies. Such phenomena include the formation of sprays and droplets, droplet coalescence and breakup, and droplet evaporation and combustion [1–4]. At subcritical conditions the droplet evaporation is well described by the classical D^2 evaporation law [5]

$$\frac{dD^2}{dt} = -\beta_v, \tag{1}$$

where β_v is the evaporation coefficient, and D is the droplet diameter. At supercritical conditions the continuum analysis of the problem is faced with suitable modeling of transport and thermodynamic properties, equations of state, and proper specification of the interface [6,7]. Using molecular dynamics simulations the modeling issues reduce to the specification of proper interatomic potentials.

Molecular dynamics simulations of nanometer-size droplets in equilibrium with a vapor have been applied for the study of the droplet pressure and density profile, and to the calculation of the surface tension as function of vapor temperature and droplet size [8–11]. Studies of non-equilibrium systems have included condensation and evaporation of argon slabs [12–14], evaporation of argon clusters [15], and evaporation of argon droplets [16,17], which recently have been extended to studies of supercritical evaporation of liquid oxygen [18]. Related molecular dynamics simulations also include studies of droplet collision cf. Svanberg et al. [19], Sikdar and Chung [20] and Murad and Law [21] and the cluster formation of a Lennard-Jones fluid during anisotropic expansion Ashurst and Holian [22].

The molecular dynamics simulations by Long, Micci, and Wong [16] involved sub-critical evaporation of an argon droplet in an argon vapor at high Knudsen numbers. At a droplet size of 5 nm (droplet consisting of 1000 atoms), they found good agreement with the theoretical correlation by assuming an evaporation coefficient of 0.3.

Little [17] simulated the sub and super-critical evaporation of nanometer-size droplets using parameters similar to the present study. For droplet sizes of 8 nm (using 5587 atoms), the evaporation coefficient was found within 20 percent of the D^2 evaporation law.

In this paper we consider the possibility of studying non-premixed combustion from the molecular level, by applying large number of molecules to approach the macro-scale physics. To validate this approach the present study involves subcritical evaporation of a droplet in a quiescent vapor allowing direct comparison with the D^2 evaporation law.

We conduct a series of high resolution simulations using several tens of thousands of computational molecules by efficiently employing tree data structures. We present a systematic convergence study to examine the influence of the different parameters imposed by the numerical method, including the size of the computational domain, cutoff radius, droplet diameter, heating frequency and size of heating region, initialisation period, and time step size. It is shown that molecular dynamics simulations converge to the D^2 evaporation law to desired accuracy by using large number of computational molecules. The paper is organized as follows: Section 2 outlines the numerical method including a description of the applied tree data structure and of the heating algorithm. Section 3 presents the convergence study and the predicted evaporation rates.

2 Molecular Dynamics

The evaporation of an argon droplet in its own vapor is studied using molecular dynamics simulations. The atoms are assumed to interact via the 12–6 Lennard-Jones pair potential

$$V(r) = 4\epsilon\left[\left(\frac{\sigma}{r}\right)^{12} - \left(\frac{\sigma}{r}\right)^{6}\right], \tag{2}$$

where r is the distance between the atoms. For argon, the zero energy distance σ is 3.4 Å, and the depth of the potential ϵ is $120k_B$, where k_B is Boltzmann's constant. The N atoms move according to Newton's law

$$m\frac{d^2\underline{r}_p}{dt^2} = -\underline{\nabla}V(\underline{r}_p), \quad p = 1, \ldots, N \tag{3}$$

and

$$\underline{\nabla}V(r_p) = \sum_{q=1}^{N} \underline{\nabla}V(|\underline{r}_p - \underline{r}_q|), \quad p = 1, \ldots, N, \tag{4}$$

where m is the mass of the atom. Numerical integration of Eq. (3) nominally requires $\mathcal{O}(N^2)$ operations, where N is the number of atoms, but is rendered an $\mathcal{O}(N)$ algorithm by the short range nature of the potential. The computational problem is reduced then to efficiently identifying the neighboring particles at each computational element. In the present work the neighbors are considered for cutoff radii of $r_c/\sigma = 2.5$, 5, and 10.

[1]Also at CTR, NASA Ames 202A-A-1, Moffett Field, CA-94035, USA.

Contributed by the Heat Transfer Division for publication in the JOURNAL OF HEAT TRANSFER. Manuscript received by the Heat Transfer Division September 10, 1999; revision received November 20, 2000. Associate Editor: T. Avedisian.

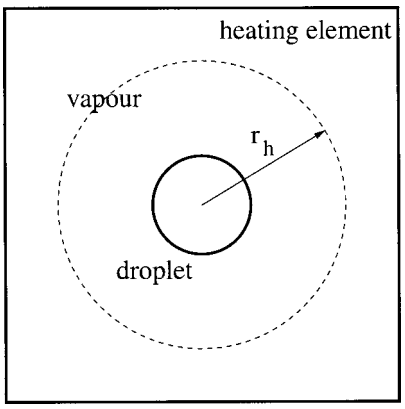

Fig. 1 Sketch of computational domain and heating element

The system of equations is integrated in time using the leap-frog scheme and a constant number of atoms and in a constant volume. Periodic boundary conditions are imposed in all spatial directions.

For a single droplet evaporating into a vapor, the far-field temperature ($\tilde{T}_v^*$) boundary condition is

$$T_v^*(r) \rightarrow \tilde{T}_v^* \quad \text{as} \quad r \rightarrow \infty, \tag{5}$$

which is enforced by a momentum scaling of the atoms located sufficiently far away from the droplet [16,23,24]. The velocity is scaled according to

$$v_i^{\text{new}} = v_i^{\text{old}} \sqrt{\frac{3T_v k_B N_h}{2E_{\text{kin}}}}, \tag{6}$$

where E_{kin} is the total kinetic energy of the N_h atoms found in the heating region ($r_i > r_h$), and r_i is the radial co-ordinate of the atom measured from the center of the computational box cf. Fig. 1. The size (r_h) of the heating element and the heating frequency are adjusted to minimize thermal noise and to obtain a good approximation of Eq. (5).

Non-dimensional quantities are marked with an asterisk and are based on σ, ϵ, k_B, and m. Specifically, time is non-dimensionalised by $\tau^* = \tau\sqrt{\epsilon/(m\sigma^2)}$. A non-dimensional time step of $\delta\tau^* = 0.005$ (≈ 10 fs) is used unless otherwise specified.

2.1 Tree Algorithm. Traditionally, molecular dynamics simulations use the Verlet neighbor list in combination with a linked list [25–27] to reduce the $\mathcal{O}(N^2)$ operations required by the direct implementation of the force evaluation cf. Eq. (4). However, for systems involving large density variations (as in the present case), the regular mesh imposed by these methods often results in inefficient load balancing on parallel computers [17,28]. The present code adopts a different strategy, by using an adaptive tree data structure to sort the atoms and to build the neighbor list. The tree is constructed at every time step by recursively dividing the computational box in eight equal sized boxes. The division of the boxes is terminated if the size of the box is less than $2r_c$, or if the number of atoms in the box is less than some prescribed value. The latter criterion allows for efficient computations of problems with large density variations. A threshold value of 40 atoms per box was used in this work. Figure 2 shows an example of a two-dimensional (quad) tree created for 16 atoms (shown as circles) using a threshold value of one atom per box. The resulting tree has four levels.

The list of neighboring boxes is constructed for each box that has no further subdivisions (childless boxes). Two boxes are said to be neighbors if they share at least one corner. The neighbor list is constructed in two steps. First, neighboring boxes at the same level in the tree (colleagues), are found for each box in the tree (a box has a maximum of 26 colleagues). The list of colleagues is

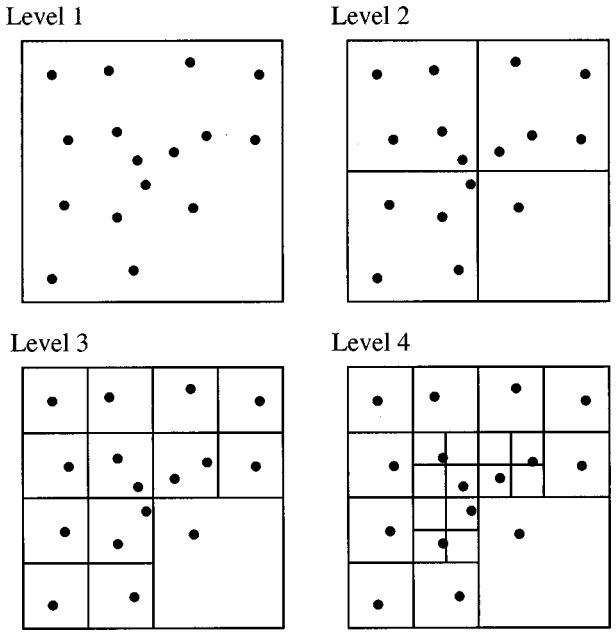

Fig. 2 Example of a two-dimensional tree created for 16 atoms and allowing one particle per box

build by traversing the tree bottom-up, starting at the next coarsest level where all (at most 8) boxes are colleagues. At higher levels of the tree the colleagues of a box are searched from the children of colleagues of the box's parent. This effectively limits the search to 6^3 boxes for each box. The colleagues (marked with an $\times$) of the shaded boxes are shown in Fig. 3. The neighbor list for the childless boxes is finally constructed by considering the colleagues and their descendents of the childless box cf. Fig. 4. The construction of the tree and the neighbor list takes less than 15 percent of the total CPU time.

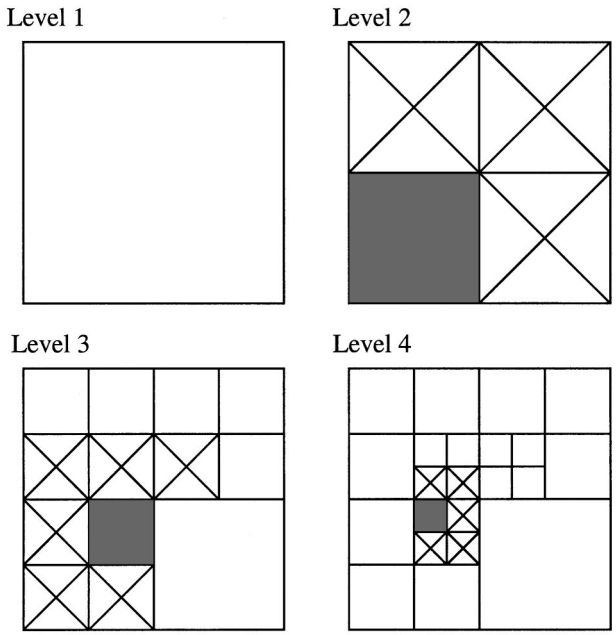

Fig. 3 Example of colleagues of boxes in the two-dimensional tree created for the 16 atoms shown in Fig. 2. The colleagues of the filled boxes are marked with an $\times$.

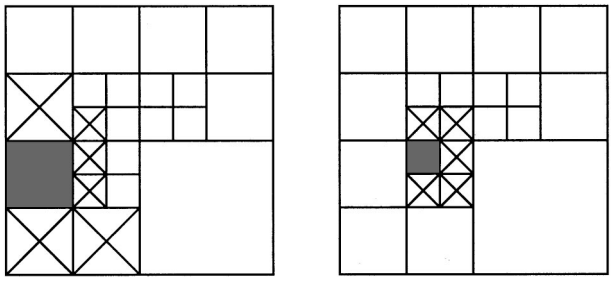

Fig. 4 Example of neighbors of boxes in the two-dimensional tree created for the 16 atoms shown in Fig. 2. The neighbors of the filled boxes are marked with an ×. The interactions of the particles in the two (filled) neighboring boxes are computed at the level of the larger box (left) utilizing the symmetry of Eq. (4).

To allow efficient computations, the atoms are mapped onto the boxes using the so called Morton ordering [29,30], in which atoms in neighboring boxes are stored in consecutive memory locations (cf. Fig. 5). This ordering can furthermore be utilized in a parallel domain decomposition of the atoms onto the processors cf. e.g. [31]. Another technique currently being investigated uses the lower levels of the tree to obtain information of the spatial distribution of the atoms and thus guiding the decomposition. After the decomposition the remaining levels of the tree can be constructed independently.

Periodic boundary conditions are handled by explicitly copying the particles in the outer regions to a ''ghost layer'' outside the computational box before the construction of the tree.

2.2 Initialization. The atoms corresponding to the liquid and vapor phases are initially placed on a face-centered-cubic (f.c.c.) lattice with a liquid and vapor density of $\rho_l^* = 0.715$ and $\rho_v^* = 0.0292$, respectively, corresponding to a non-dimensional saturation temperature of $T_{\text{sat}}^* = 0.83$ cf. [32]. The droplet is ''cut'' from the cubic f.c.c. lattice into a spherical shape to reduce the required relaxation period.

The atoms are assigned a Maxwellian velocity distributed with the desired initial temperature ($T_l^* = T_v^* = T_{\text{sat}}^*$) corresponding to a saturation pressure of $p^* = 0.0076$ and well below the critical pressure for argon of $p_{\text{crit}}^* = 0.1154$ cf. [33]. At these conditions the droplet will be in equilibrium with the surrounding vapor. The initial mean drift velocity is computed and subtracted accordingly.

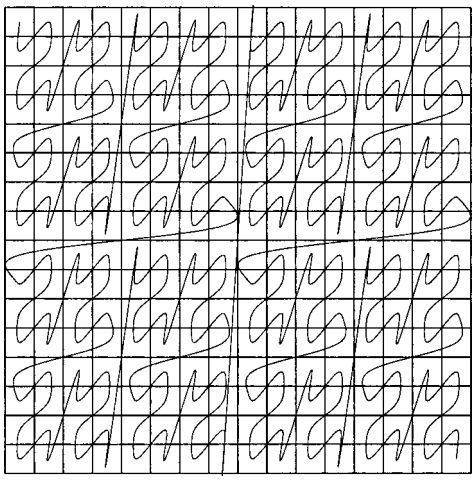

Fig. 5 Atoms in neighboring boxes are stored in consecutive memory locations to allow efficient computations using Morton ordering

Table 1 List of spatial systems investigated. $D^* = D/\sigma$ is the initial droplet diameter, $L^* = L/\sigma$ is size of the computational domain, N_{drop} and N_{vapor} are the initial number of atoms in the droplet and vapor phases respectively. $\alpha = L/D$ is the relative size of the computational domain, and $r_h^* = r_h/\sigma$ the position of the heating element.

System	D^*	L^*	N_{drop}	N_{vapour}	α	r_h^*
I	22	77	5768	13260	6	25
II	22	87	5768	19316	7	25
III	22	103	5768	31664	8	25
IV	38	113	22360	41432	6	30
V	51	155	51105	105480	6	40

The system is subsequently relaxed for 25 or 50 non-dimensional time units by heating the complete system to a temperature of 0.83 at every $\tau_h/\delta\tau$ time step, where $1/\tau_h$ is the heating frequency. During this initial heating the change in droplet diameter is less than 2 percent confirming that the droplet is in equilibrium with the surrounding vapor. After the relaxation, the temperature of the ''far-field'' vapor atoms is increased to the desired value of $T_v^* = 2.5$.

The size of the computational box ($L \times L \times L$) is chosen sufficiently large to avoid large density and pressure increases during the evaporation, and to accommodate the temperature far-field boundary condition. Using a non-dimensional box size of ($\alpha \equiv L/D$) 6 to 8, where D is the droplet diameter results in pressure rises of 0.012 to 0.0285 (15–40 percent pressure increase), which are both well below p_c^*.

Five spatial systems are investigated including three different droplet diameters ($D = 8$, 13, and 17 nm) and three different sizes of the computational domain cf. Table 1. The number of atoms range from 5769 and 13260 to 51105 and 105480 for the liquid and vapor phases, respectively. In all the cases, the heating was performed on atoms located well beyond the region of the droplet ($r_h/\sigma > 25$, 30, and 40).

2.3 Diagnostics. The density and temperature profiles presented in the following are instantaneous profiles obtained by sampling the enumeration of atoms and the associated kinetic energy in concentric shells of constant radial spacing around the system's center of mass. A total of fifty shells were found to give a good resolution of the extracted fields.

The size of the droplet is given by the number of atoms found in the liquid phase as [17]

$$D^2 \approx \left(6 \frac{N_{\text{drop}} m}{\pi \rho_l} \right)^{2/3}, \tag{7}$$

where a spherical shape has been assumed. Using a simple Cartesian binning of the atoms, and assigning atoms in bins with a sufficiently high density to the liquid phase was found to give insufficient resolution. Instead, the local density is computed at the position of each atom using a spherical binning. A radius of interrogation of $1.5r_c$ provides sufficient statistics while at the same time retaining the spatial resolution. Atoms with a local density exceeding a threshold density (ρ_c^*) are assigned to the liquid phase. The threshold value was found to determine the size of the drop to within a constant and hence not to influence the predicted evaporation rate. Thus, using a fixed value of ρ_c^*

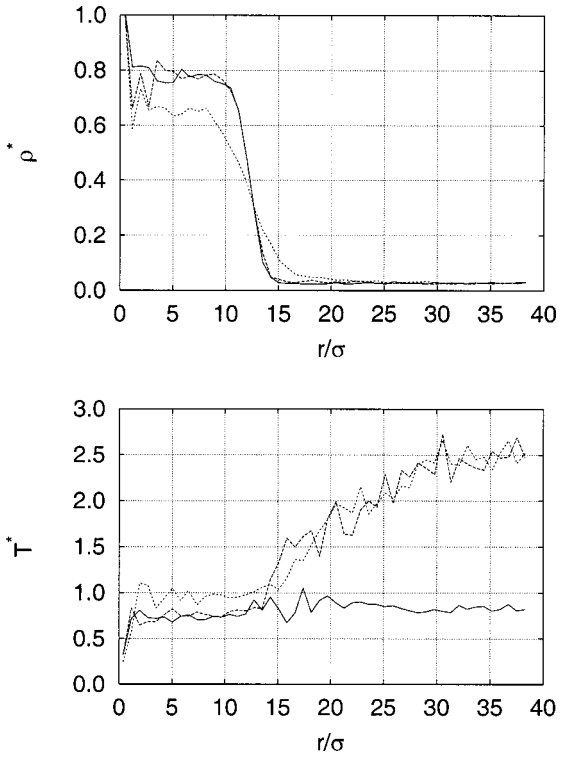

Fig. 6 Droplet density and temperature profiles during accommodation and evaporation of the 5768 atom droplet (Case E01). (—: $\tau^*=25$; – – –: $\tau^*=30$; - - -: $\tau^*=100$)

$=0.298$, and applying this procedure to the initial f.c.c. lattice resulted in deviations in number of liquid atoms of less than 3 percent.

2.4 Evaporation. After the initial relaxation, the reduced temperature of the vapor is raised to 2.5 corresponding to a pressure of 0.071. The droplet is heated by the vapor until the saturation temperature is reached at $T^*=1.156$, when the droplet starts to evaporate. The radial density and temperature profiles during heating and evaporation at $\tau^*=25$, 30, and 100 are shown in Fig. 6 for Case I. At $t^*=30$ the center of the droplet is seen to be slightly sub-cooled at a temperature of 0.83.

At these subcritical conditions the droplet is expected to evaporate according to the D^2 evaporation law (1)

$$\frac{d(D^2)}{dt}=-\beta_v,$$

where the evaporation coefficient β_v is given by [5]

$$\beta_v=\left(\frac{8\rho_s\mathcal{D}_s}{\rho_l}\right)\ln(1+B), \tag{8}$$

where ρ_s and $\mathcal{D}_s$ are the density and self-diffusion at the surface of the droplet. The transfer number B is

$$B=\frac{c_p(T_v-T_s)}{h_{fg}}, \tag{9}$$

where c_p and h_{fg} are the specific heat and heat of vaporization, and T_v and T_s are the temperature of the vapor and the droplet surface temperature, respectively. The coefficient of self-diffusion is found from [34]

$$\mathcal{D}=2.6280\times10^{-22}\frac{\sqrt{T_v^3/M}}{p_v\sigma^2\Omega^{(1,1)^*}(T_v^*)}, \tag{10}$$

where p_v is the vapor pressure, M the molar mass, and $\Omega^{(1,1)*}$ the collision integral.

Since $(\rho\mathcal{D})$ varies slowly with temperature, $(\rho_v\mathcal{D}_v)$ can replace $(\rho_s\mathcal{D}_s)$, and $\mathcal{D}_v$ is the self-diffusion of the vapor. Using the parameters for argon ($c_p=548$ J/kg K, and $h_{fg}=88$ kJ/kg) [32], and $(\Omega^{(1,1)*}=0.996)$ [34] the transfer number is close to unity and the diffusion coefficient is 623×10^{-9} m^2/s.

The self-diffusion coefficient of the bulk vapor has also been computed in separate equilibrium molecular dynamics simulations for system sizes of 1372 and 2916 atoms, respectively. The self-diffusion is computed from the Green-Kubo relation [26]

$$\mathcal{D}=\frac{1}{3N}\int_0^\infty\sum_j^N \underline{v}_j(t)\cdot\underline{v}_j(0)\,dt, \tag{11}$$

where $\underline{v}_j(t)$ is the velocity of the jth atom at time t. The predicted values are 592×10^{-9} m^2/s and 639×10^{-9} m^2/s for the two system sizes and within 5 percent of the theoretical value given by Eq. (10).

3 Results

A range of simulations were conducted to study the consistency and convergence of the MD approach and to determine the influence of the cutoff radius, the temporal and spatial resolution, and the heating frequency. The list of simulations is shown in Table 2, and the computational cost for each case is listed in Table 2. The present tree code was compared with a traditional cell index code for System I and V using cutoff values of 2.5 and 5.0, respectively. The cell index was found to be 20–30 percent faster for the smaller cutoff value and for the smaller system (System I), whereas the tree code is approximately 40 percent faster for the larger system (System V) using a cut-off value of 5.0. The comparison was performed on a SGI (Octane R10k) workstation. During the simulations the droplet remained close to the geometrical center of the computational box, and hence no drift adjustment was required.

3.1 Convergence Study. The sensitivity of the different numerical parameters is studied for the radial density and temperature profiles during the evaporation of the 5766 atom droplet.

3.1.1 Spatial Convergence. Simulations are conducted to study the influence of the cutoff radius using $r_c/\sigma=2.5$, 5.0, and 10.0, respectively. The influence on the non-dimensional radial density and temperature profiles at a non-dimensional time of 200 is shown in Fig. 7. The simulation using the smaller cutoff radius $(r_c/\sigma=2.5)$ clearly exhibits increased evaporation and lower droplet density due to the discontinuous cutoff of the potential and the reduced surface tension [35]. The mean difference between the simulation using a cutoff radius of 2.5 and the simulations using higher cutoff value is 12 percent, whereas the difference between the simulations of 5.0 and 10.0 is less than 1.0 percent. Similar but less severe trends can be observed in the temperature profile (Fig. 7) exhibiting difference less than 1.0 percent between the simulations.

Three different sizes of the computational box, $\alpha=6$, 7, and 8 are tested, and differences of 2.9 percent and 5.3 percent are observed in the temperature profiles for a non-dimensional time of 100 and 200, respectively (not shown). The corresponding deviations in the density profiles are less than 0.5 percent, consistent with a prediction of the evaporation rate that is insensitive to α.

3.1.2 Temporal Convergence. The temporal convergence is studied using different non-dimensional time step sizes of 0.005 (Case E01) and 0.010 (Case E08), respectively. The differences in both the density and temperature profiles are less than 1.7 percent (not shown). Similar deviations are observed for the length of the initialization period (Cases E01 and E09 using 25 and 50 non-dimensional time units, respectively). The effect of doubling the

Table 2 List of simulation cases. The "system" refers to the spatial systems listed in Table 1, r_c/σ is the cutoff radius, $\alpha = L/D$ the size of the computational box, $\delta\tau^*$ the non-dimensional time step, $\tau_h/\delta\tau$ the heating frequency, $\tau_i/\delta\tau$ the initialization period, CPU time per time step (in seconds on a Sun Ultra 2 workstation), and β_v is the predicted evaporation rate. The theoretical evaporation rate is 1.7×10^{-7} m^2/s.

Case	System	r_c/σ	α	$\delta\tau^*$	$\tau_h/\delta\tau$	$\tau_i/\delta\tau$	CPU time	β_v
E01	I	2.5	6	0.0050	100	5000	1.0	1.43×10^{-7}
E02	I	5	6	0.0050	100	5000	1.2	1.13×10^{-7}
E03	I	10	6	0.0050	100	5000	3.8	1.13×10^{-7}
E04	II	2.5	7	0.0050	100	5000	-	1.43×10^{-7}
E05	III	2.5	8	0.0050	100	5000	-	1.43×10^{-7}
E06	IV	2.5	6	0.0050	100	5000	-	1.76×10^{-7}
E07	V	2.5	6	0.0050	100	5000	-	1.78×10^{-7}
E08	I	2.5	6	0.0100	50	2500	-	-
E09	I	2.5	6	0.0050	100	10000	-	-
E10	I	2.5	6	0.0050	500	5000	-	-
E11	I	2.5	6	0.0050	1000	5000	-	-

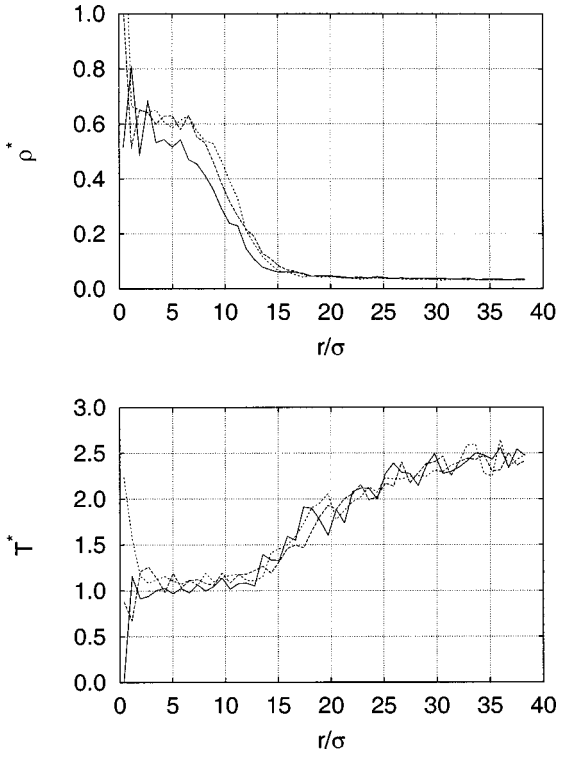

Fig. 7 Convergence of the density and temperature profiles as function of the cutoff radius for the 5768 droplet at $\tau^*=200$. —: $r_c/\sigma=2.5$ (Case E01); – – –: $r_c/\sigma=5.0$ (Case E02); - - -: $r_c/\sigma=10.0$ (Case E03)

initialization period results in a difference in the profiles of less than 1.7 percent (not shown). Thus, an initialization period of 25 is used throughout.

3.1.3 Heating Frequency. The effect of the heating frequency ($1/\tau_h$) is studied using three different heating rates: $\tau_h/\delta\tau = 100$, 500, 1000 (Cases: E01, E10, and E11), and the difference in the density and temperature profiles are found to be less than 0.5 percent and 1.3 percent, respectively. One simulation was conducted to study the initial heat contents of the system. In this

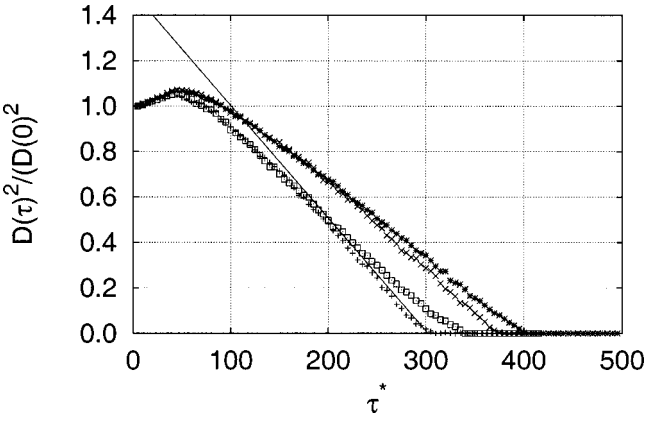

Fig. 8 Evaporation curve for the 5768 droplet. +: E01 ($r_c/\sigma=2.5$); ×: E02 ($r_c/\sigma=5.0$);*: E03 ($r_c/\sigma=10.0$); □: E05 ($r_c/\sigma=2.5$); —: Theory.

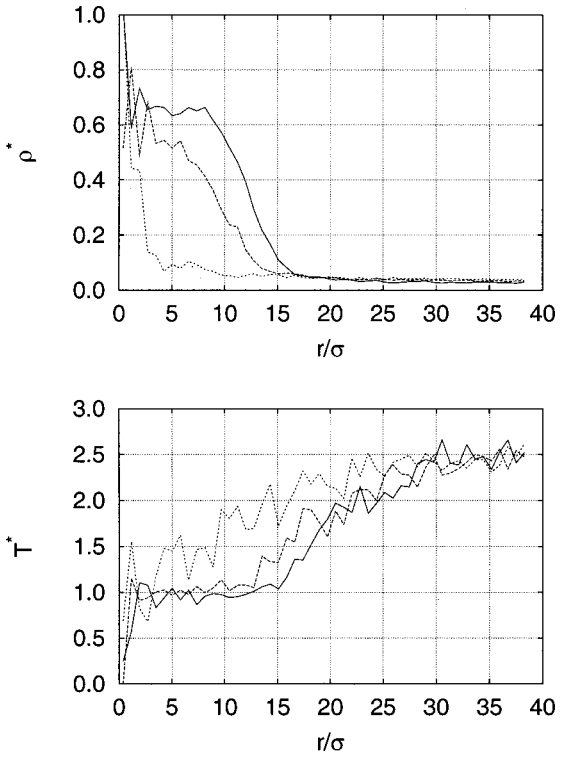

Fig. 9 Density and temperature profiles during evaporation for the 5867 atom droplet (Case E02). —: $\tau^*=100$; – – –: $\tau^*=200$; - - -: $\tau^*=300$.

case the heating was stopped after the initialization and the droplet reached an equilibrium with a radius close to the initial.

3.2 Evaporation Coefficient. The non-dimensional evaporation rate (D^2/D_0^2) for the 5867 atom droplet simulation is shown in Fig. 8 for the different cutoff values. D_0 is the initial droplet diameter. The initial relaxation during the first 25 non-dimensional time units, and the subsequent heating of the droplet including condensation of vapor on the droplet [36], is clearly visible until $\tau^* \approx 100$. As the droplet reaches saturation, the evaporation follows the D^2 evaporation law.

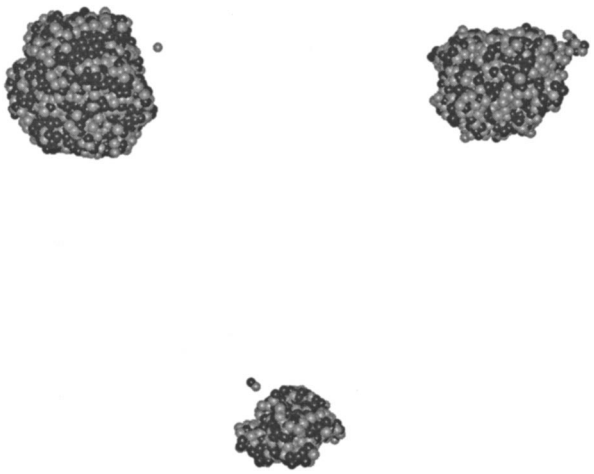

Fig. 10 Time history of the 5867 atom droplet during evaporation (Case E02) (vapor not shown). From left to right: $\tau^*=100$, 200, and 300.

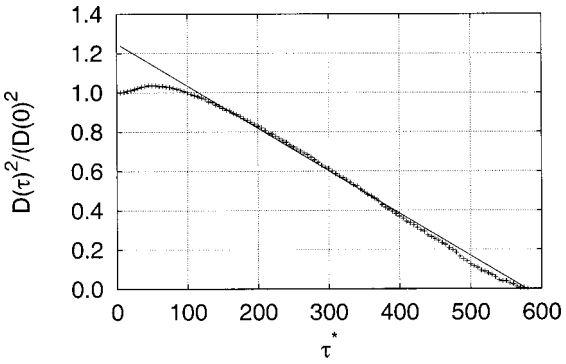

Fig. 11 Evaporation curve for the 22360 atom droplet. +: E06; —: Theory.

The ''numerical'' heating and evaporation caused by the discontinuous cutoff of the potential is seen for the simulations E01 and E05 as compared to the E02 and E03 cases.

Using Eq. (8) and a mean liquid density of 0.6, see e.g., Fig. 7 gives a theoretical evaporation coefficient of 1.7×10^{-7} m^2/s. The simulated values extracted from Fig. 8 are 1.43×10^{-7} m^2/s and 1.13×10^{-7} m^2/s for the small and large cutoff simulation (cf. Table 2). Hence, the predicted evaporation coefficients are within

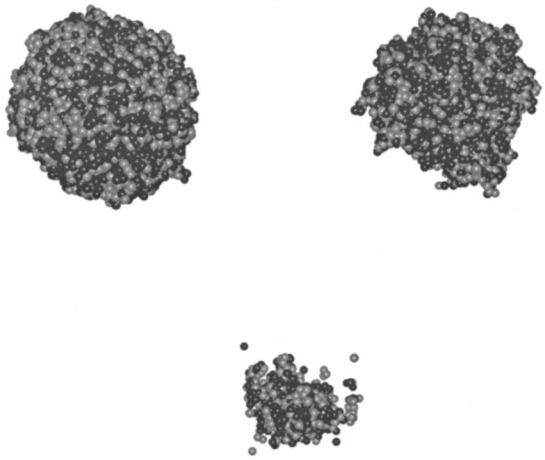

Fig. 12 Time history of the 22360 atom droplet during evaporation (vapor not shown). From left to right: $\tau^*=100$, 300, and 500.

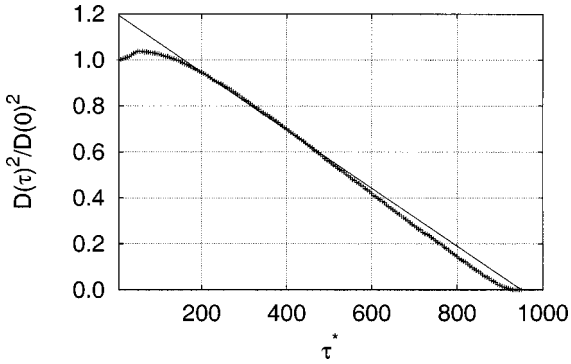

Fig. 13 Evaporation curve for the 51104 atom droplet. +: E07; —: Theory.

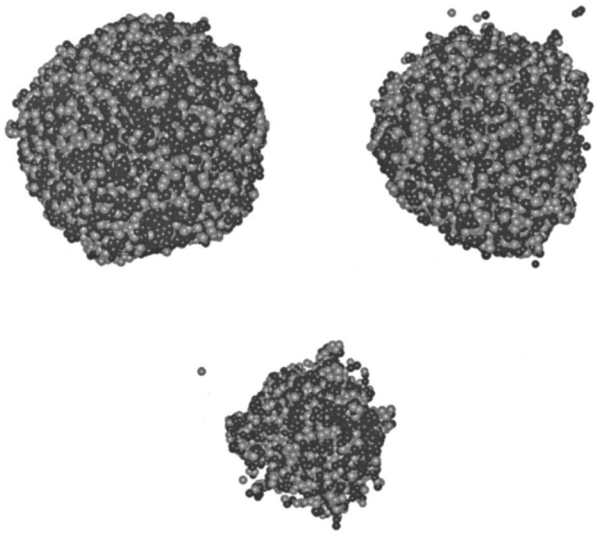

Fig. 14 Time history of the 51104 droplet during evaporation. From left to right: $\tau^*=100$, 400, and 700.

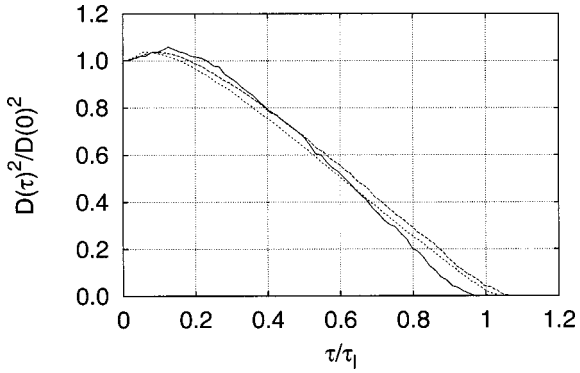

Fig. 15 Evaporation rate. —: 5678 atom droplet; – – –: 22310 atom droplet; - - -: 51104 atom droplet.

16 percent to 34 percent of the theoretical value. Deviations of the same magnitude were also found by Little [17], using similar number of atoms.

The corresponding radial density and temperature profiles are shown in Fig. 9. The instantaneous position of the liquid atoms during evaporation (Case E02) as determined from the local density method is shown in Fig. 10. Atoms originally in the vapor or liquid phases are coloured light gray and black, respectively. The atoms are plotted in scale as spheres with a radius of σ.

Higher resolution simulations were run in order to establish the convergence of the method with respect to theoretically predicted values. The evaporation curve, density and temperature profiles, and snapshots for the 22360 and 51104 atom droplets are shown in Figs. 11–12 and 13–14, respectively. The simulated evaporation coefficients are 1.76×10^{-7} m^2/s and 1.78×10^{-7} m^2/s cf. Table 2, both in excellent agreement with the theoretical value. Thus, the simulations converge to the theoretical values as the number of droplet atoms is increased beyond 10^4.

To combine the evaporation curves for the different droplet sizes, time is non-dimensionalized using the macro-scale droplet life time,

$$\tau_l=\frac{\beta_v}{D_0^2}. \tag{12}$$

where D_0 is the initial droplet diameter extrapolated from Figs. 8, 11, and 13. The evaporation rate consequently collapses as shown in Fig. 15.

4 Conclusion

The sub-critical evaporation of a nanometer-size droplet has been simulated using the method of molecular dynamics. The far-field boundary condition for the temperature is implemented by a regional heating technique, allowing correct prescription of far-field conditions.

An adaptive tree data structure is employed to sort the particles and to build the neighbor lists in order to reduce the computational cost. The efficiency is further enhanced by mapping the particles consecutively in memory using Morton ordering.

Convergence of the method has been demonstrated by varying the numerical parameters such as droplet size, domain size, cutoff range, time step size, initialisation length, and heating frequency.

Three argon droplets with diameters of approximately 8, 13, and 17 nm corresponding to 5768, 22360, and 51105 liquid atoms, respectively, were evaporated into an argon vapor at a non-dimensional temperature of 2.5 and a pressure of 0.071. For the 8 nm droplet, the evaporation rate was found within 35 percent of the theoretical predictions, whereas the evaporation rate of the two larger droplets deviated less than 5 percent.

In the investigated parameter range, the largest differences were observed for the simulations using different cutoff values resulting in increasing the evaporation rate for the smaller cutoff values.

The results of the simulations demonstrate that molecular dynamics simulations can be a consistent numerical method for the simulation of thermodynamics of nano-scale phenomena. New computational techniques and algorithms allow us to conduct routine calculations using tens of thousands and hundred of thousands of atoms, thus reaching more realistic behavior of the system being simulated.

Nomenclature

Greek

α = non-dimensional box size
β_v = evaporation coefficient
$\delta\tau$ = non-dimensional time step
ϵ = energy scale of Lennard-Jones potential
ρ = density
σ = zero energy distance of Lennard-Jones potential
τ = time
τ_l = droplet life time
τ_h = heating time interval
$\Omega^{(1,1)}$ = collision integral

Roman

B = transfer number
$\mathcal{D}$ = self-diffusion coefficient
$\mathcal{D}_s$ = self-diffusion coefficient at the surface of the droplet
$\mathcal{D}_v$ = self-diffusion coefficient of the vapor
D = droplet diameter
E_{kin} = kinetic energy
L = size of computational box
N = total number of atoms
N_h = number of atoms in heating region
N_{drop} = number of atoms in the droplet
T = temperature
V = potential
c_p = specific heat
h_{fg} = heat of vaporisation
k_B = Boltzmann's constant
m = atomic mass
r = distance
r_c = cutoff radius
r_h = distance from center of box to heating region

r_i = distance from center of box to i-th atom
p = pressure
v = velocity
T = temperature
T_{sat} = saturation temperature
t = time

Superscripts

* = non-dimensional quantity

Subscripts

0 = initial value
crit = critical
v = vapor
l = liquid
c = cutoff
h = belonging to heating region
i = initialisation
sat = saturation

References

[1] Glassman, I., 1994, ''A Look Forward: The Next 25 Years,'' Combust. Sci. Technol., **98**, pp. 217–222.
[2] Brezinsky, K., 1994, ''The Next Twenty Five Years of Combustion Research: One Researcher's Perspective,'' Combust. Sci. Technol., **98**, pp. 237–243.
[3] Sirignano, W. A., 1993, ''Fluid Dynamics of Sprays—1992 Freeman Scholar Lecture,'' J. Fluids Eng., **115**, pp. 345–378.
[4] Aggarwal, S. K., and Peng, F., 1995, ''A Review of Droplet Dynamics and Vaporization Modeling for Engineering Calculations,'' ASME J. Eng. Gas Turbines Power, **117**, pp. 453–461.
[5] Kuo, K. K.-Y., 1986, *Principles of Combustion*, John Wiley & Sons, New York.
[6] Shuen, J. S., Yang, V., and Hsiao, C. C., 1992, ''Combustion of Liquid-Fuel Droplets in Supercritical Conditions,'' Combust. Flame, **89**, pp. 299–319.
[7] Yang, V., Lin, N. N., and Shuen, J.-S., 1994, ''Vaporization of Liquid Oxygen (LOX) Droplets in Supercritical Hydrogen Environments,'' Combust. Sci. Technol., **97**, pp. 247–270.
[8] Protsenko, S. P., and Skripov, V. P., 1977, ''Molecular-Dynamics Calculation of Thermodynamic Properties and Structure System of Liquid Argon Nuclei,'' Sov. J. Low Temp. Phys., **3**, No. 1, pp. 1–4.
[9] Rusanov, A. I., and Brodskaya, E. N., 1977, ''The Molecular Dynamics Simulation of a Small Drop,'' J. Colloid Interface Sci., **62**, No. 3, pp. 542–555.
[10] Powles, J. G., Fowler, R. F., and Evans, W. A. B., 1983, ''A New Method for Computing Surface Tension Using a Drop of Liquid,'' Chem. Phys. Lett., **96**, No. 3, pp. 289–292.
[11] Thompson, S. M., Gubbins, K. E., Walton, J. P. R. B., Chantry, R. A. R., and Rowlinson, J. S., 1984, ''A Molecular Dynamics Study of Liquid Drops,'' J. Chem. Phys., **81**, No. 1, pp. 530–542.
[12] Yasuoka, K., Matsumoto, M., and Kataoka, Y., 1994, ''Evaporation and Condensation at a Liquid Surface of Argon,'' J. Chem. Phys., **101**, No. 9, pp. 7904–7911.
[13] Matsumoto, M., 1996, ''Molecular Dynamics of Liquid Surfaces,'' Mol. Simul., **16**, pp. 209–217.
[14] Zhakhovskiĭ, V. V., and Anisimov, S. I., 1997, ''Molecular-Dynamics Simulation of Evaporation of a Liquid,'' JETP, **84**, No. 4, pp. 734–745.
[15] Rytkönen, A., Valkealahti, S., and Manninen, M., 1997, ''Melting and Evaporation of Argon Clusters,'' J. Chem. Phys., **106**, No. 5, pp. 1888–1892.
[16] Long, L. N., Micci, M. M., and Wong, B. C., 1996, ''Molecular Dynamics Simulations of Droplet Evaporation,'' Comput. Phys. Commun., **96**, pp. 167–172.
[17] Little, J. K., 1996, ''Simulation of Droplet Evaporation in Supercritical Environments Using Parallel Molecular Dynamics,'' Ph.d. thesis, The Pennsylvania State University.
[18] Kaltz, T. L., Long, L. N., Micci, M. M., and Little, J. K., 1998, ''Supercritical Vaporization of Liquid Oxygen Droplets Using Molecular Dynamics,'' Combust. Sci. Technol., **136**, pp. 279–301.
[19] Svanberg, M., Marković, N., and Petterson, J. B. C., 1998, ''Collision Dynamics of Large Water Clusters,'' J. Chem. Phys., **108**, No. 14, pp. 5888–5897.
[20] Sikdar, S., and Chung, J. N., 1997, ''A Quasimolecular Approach for Discrete Study of Droplet Collision,'' Int. J. Comput. Fluid Dyn., **8**, pp. 189–200.
[21] Murad, S., and Law, C. K., 1999, ''Molecular Simulation of Droplet Collision in the Presence of Ambient Gas,'' Mol. Phys., **96**, No. 1, pp. 81–85.
[22] Ashurst, W. T., and Holian, B. L., 1999, ''Droplet Size Dependence Upon Volume Expansion Rate,'' J. Chem. Phys., **111**, No. 6, pp. 2842–2843. (Letters to the Editor).
[23] Grönbeck, H., Tománek, D., Kim, S. G., and Rosén, A., 1997, ''Does Hydrogen Pre-Melt Palladium Clusters?,'' Chem. Phys. Lett., **264**, pp. 39–43.
[24] Westergren, J., Grönbeck, H., Kim, S.-G., and Tománek, D., 1997, ''Noble Gas Temperature Control of Metal Clusters: A Molecular Dynamics Study,'' J. Chem. Phys., **107**, No. 8, pp. 3071–3079.
[25] Verlet, L., 1967, ''Computer Experiments on Classical Fluids,'' Phys. Rev., **159**, pp. 98–103.
[26] Allen, M. P., and Tildesley, D. J., 1987, *Computer Simulation of Liquids*, Clarendon Press, Oxford.
[27] Grest, G. S., and Dünweg, B., 1989, ''Vectorized Link Cell FORTRAN Code for Molecular Dynamics Simulations for a Large Number of Particles,'' Comput. Phys. Commun., **55**, pp. 269–285.
[28] Plimpton, S., 1995, ''Fast Parallel Algorithms for Short-Range Molecular Dynamics,'' J. Comput. Phys., **117**, pp. 1–19.
[29] Samet, H., 1989, *The Design and Analysis of Spatial Data Structures*, Addison-Wesley Publishing Company.
[30] Cottet, G.-H., and Koumoutsakos, P., 2000, *Vortex Methods: Theory and Practice*, Cambridge University Press, New York.
[31] Salmon, J. K., and Warren, M. S., 1993, ''Skeletons From the Treecode Closet,'' J. Chem. Phys., **111**, pp. 136–155.
[32] Rabinovich, V. A., Vasserman, A. A., Nedostup, V. I., and Veksler, L. S., 1988, *Thermophysical Properties of Neon, Argon, Krypton, and Xenon*, Hemisphere.
[33] Reynolds, W. C., 1979, *Thermodynamic Properties in SI*, Stanford University.
[34] Hirschfelder, J. O., Curtiss, C. F., and Bird, R. B., 1967, *Molecular Theory of Cases and Liquids*, 4th ed., John Wiley & Sons, New York.
[35] Mecke, M., Winkelmann, J., and Fischer, J., 1997, ''Molecular Dynamics Simulation of the Liquid-Vapor Interface: The Lennard-Jones Fluid,'' J. Chem. Phys., **107**, No. 21, pp. 9264–9270.
[36] Margerit, J., and Sero-Guillaume, O., 1996, ''Study of the Evaporation of a Droplet in Its Stagnant Vapor by Asymptotic Matching,'' Int. J. Heat Mass Transf., **39**, No. 18, pp. 3887–3898.